EPJ Web of Conferences **346**, 01023 (2026) https://doi.org/10.1051/epjconf/202634601023
RFPPC2025

An implicit-explicit time splitting strategy for the far SOL plasma fluid model with DG-FEM discretization

Olena Burkovska[1,*], *Rhea L.* Barnett[2], *Christopher J.* Vogl[3], *Jeremy D.* Lore[2], and *Cory* Hauck[1]

[1]Computer Science and Mathematics Division, Oak Ridge National Laboratory, Oak Ridge, TN, USA
[2]Fusion Energy Division, Oak Ridge National Laboratory, Oak Ridge, TN, USA
[3]Center for Applied Scientific Computing, Lawrence Livermore National Laboratory, Livermore, CA, USA

Abstract. We consider a far scrape-off layer (SOL) plasma fluid model of ions that is governed by a Braginskii-type model: a one-dimensional, nonlinear system of advection-diffusion equations coupled with a diffusion equation for neutral particles. Our motivation for studying this system arises from the coupling between the edge plasma and radio-frequency (RF) heating, where solving a far SOL plasma fluid model provides critical insights into edge plasma dynamics. Numerical simulations of plasma fluid models require advanced computational techniques to achieve both efficiency and accuracy, especially when resolving the boundary layer in magnetically confined plasmas. In this work, we propose an implicit-explicit time operator splitting strategy that allows for an efficient solution algorithm, where the diffusive terms are treated semi-implicitly requiring only a linear solve, while the advection part is handled explicitly using a strong-stability-preserving Runge-Kutta (SSP-RK3) scheme. This leads to a fully decoupled system in which the diffusion and advection sub-problems can be solved separately, simplifying the overall solution procedure and allowing for efficient parallelization, which is particularly relevant for exploring the impact of RF heating on the SOL plasma. The main challenge of the discretization is due to the strong coupling between diffusion and advection, particularly through the boundary conditions. This makes implementation of such a scheme in an accurate and stable manner nontrivial. We discuss in detail how to split the equations and manage boundary conditions to maintain stability and well-posedness for each subsystem. We also describe a spatial discretization approach, based on the discontinuous Galerkin finite element method (DG-FEM) and present numerical results for a one-dimensional system.

1 Introduction

The plasma boundary region of a magnetic confinement fusion device exhibits many complex physical processes, including plasma turbulence, localized power deposition, gas fueling and impurity seeding, and strong plasma-neutral interactions. A large number of transport solvers have been developed to model this scrape-off layer (SOL) region, with an important class being fluid plasma codes that can advance the transport equations on equilibrium timescales. These codes, such as SOLPS-ITER [1, 2], EMC3-EIRENE, UEDGE [3], EDGE2D [4], and SolEdge-HDG [5, 6], do not resolve plasma turbulence, but instead take user-defined diffusivities and convective velocities as input to represent transport in the cross-field direction. Additionally, the magnetic field is considered to change on a timescale much slower than the plasma transport. The plasma-neutral and plasma-surface interactions, on the other hand, are typically treated with a relatively high fidelity, and the SOL is well represented. Therefore, these codes are routinely used to interpret existing experimental results and inform the design of linear, tokamak, and stellarator devices around the world [7–11].

Radio-frequency (RF) wave power is routinely used to heat magnetically confined fusion plasmas. Modification of the plasma profiles is observed during RF operation, especially in the far-SOL close to the actuators [12–18]. Therefore, it is critical to have robust plasma solvers in this region, both for the equilibrium transport and RF wave propagation. However, implementing boundary conditions in a fluid transport code that provide stable solutions at any plasma facing component (PFC) - plasma interface can be challenging as the boundary condition required on the parallel velocity $u_{\|} \geq c_s$, where c_s is the sound speed, can exhibit inconsistencies due to its derivation based on kinetic models [19, 20].

We present a detailed analysis of a Braginskii-like system of fluid plasma transport equations, with a particular focus on setting appropriate boundary conditions, to facilitate a deeper understanding of the physics in this region. We also present a detailed space-time discretization, based on an efficient implicit-explicit operator splitting scheme with a discontinuous Galerkin (DG) method for spatial discretization. By treating diffusion semi-implicitly and

*Corresponding author: burkovskao@ornl.gov This manuscript has been authored in part by UT-Battelle, LLC, under contract DE-AC05-00OR22725 with the US Department of Energy (DOE). The publisher acknowledges the US government license to provide public access under the DOE Public Access Plan (http://energy.gov/downloads/doe-public-access-plan). This work was also performed in part under the auspices of the U.S. Department of Energy by Lawrence Livermore National Laboratory under Contract DE-AC52-07NA27344, LLNL-PROC-2007576.

advection explicitly, the method enables stable, decoupled time integration and can facilitate efficient parallel computations.

The paper is organized as follows: Section 2 introduces the Braginskii-like fluid model. Section 3 presents the implicit-explicit operator splitting scheme used for time integration. Section 4 describes the spatial discretizations with details on the numerical treatment of boundary fluxes. Section 5 focuses on the analysis and implementation of boundary conditions. Finally, Section 6 provides numerical results that illustrate our study.

2 Model problem: Parallel advection-diffusion in one dimension

We consider a one-dimensional version of Braginskii type equations [21] for continuity, ion parallel momentum in a direction parallel to the magnetic field and neglecting the perpendicular transport. Given a computational domain $\Omega = [0, L]$, where $x = 0$ is the plasma reflection point and $x = L$ the device wall, we consider the following system

$$
\begin{aligned}
&\frac{\partial}{\partial t} n_0 + \frac{\partial}{\partial x}\left(-D_0 \frac{\partial}{\partial x} n_0\right) = -S^n,\\
&\frac{\partial}{\partial t} n + \frac{\partial}{\partial x}(nu) = S^n,\\
&\frac{\partial}{\partial t}(m_i n u) + \frac{\partial}{\partial x}\left(m_i n u^2 - m_i n \mu \frac{\partial}{\partial x} u + n(T_e + T_i)\right) = S^m,\\
&\frac{\partial}{\partial t}\Big(\frac{3}{2} n T_i + \frac{1}{2} m_i n u^2\Big) + \frac{\partial}{\partial x}\Big[\Big(\frac{5}{2} n T_i + \frac{1}{2} m_i n u^2\Big) u - n\chi_i \frac{\partial}{\partial x} T_i\Big]\\
&\quad = S_i^E + S_i^{E,ext},\\
&\frac{\partial}{\partial t}\Big(\frac{3}{2} n T_e\Big) + \frac{\partial}{\partial x}\Big(\frac{5}{2} n T_e u - n\chi_e \frac{\partial}{\partial x} T_e\Big) = S_e^E + S_e^{E,ext},
\end{aligned}
\tag{2.1}
$$

where we have dropped the $||$ subscript for u and have assigned x the parallel coordinate. Here, n_0, n, u, $T_{i,e}$ are the neutral density, plasma density, velocity, ion and electron temperatures, respectively. We also denote $q = nu$, $E_e = \frac{3}{2} n T_e$, $E_i = \frac{3}{2} n T_i + \frac{1}{2} m_i n u^2$, $p_{i,e} = n T_{i,e}$ to be the momentum, ion and electron energies and pressures, respectively. Here, D_0 , μ, and χ are the collisional coefficients (units m^2/s) for particle diffusion, viscosity, and heat diffusion for the density, momentum, and energy equations respectively; the source terms, $S^{n,m,E}$, contain any contributions from e.g., cross-species collisions, and plasma-neutral interactions; and $S_{i,e}^{E,ext}$ are the external heat sources (e.g., RF heating). Cross-field drifts, impurity ions, and plasma current are neglected. The units are SI except for temperature (eV) and the diffusion coefficients are defined as follows

$$
\begin{aligned}
D_0 &= 8T_0 / \left(3\pi m_0 n (\langle\sigma v\rangle_{iz} + \langle\sigma v\rangle_{cx})\right),\\
\mu &= \frac{0.96 T_i \tau_i}{m_i} = \frac{0.96}{\sqrt{m_i}} \frac{3(4\pi\epsilon_0)^2}{4\sqrt{\pi}\ln\Lambda e^4 Z^4}\left(T_i^{5/2}/n\right),\\
\chi_i &= \frac{3.9 T_i \tau_i}{m_i} = \frac{3.9}{\sqrt{m_i}} \frac{3(4\pi\epsilon_0)^2}{4\sqrt{\pi}\ln\Lambda e^4 Z^4}\left(T_i^{5/2}/n\right),\\
\chi_e &= \frac{3.16 T_e \tau_e}{m_e} = \frac{3.16}{\sqrt{m_e}} \frac{3(4\pi\epsilon_0)^2}{4\sqrt{2\pi}\ln\Lambda e^4 Z^2}\left(T_e^{5/2}/n\right),\\
\tau_i &= \frac{(4\pi\epsilon_0)^2 3\sqrt{m_i} T_i^{3/2}}{4\sqrt{\pi}\ln\Lambda e^4 Z^4 n},\ \tau_e = \frac{(4\pi\epsilon_0)^2 3\sqrt{m_e} T_e^{3/2}}{4\sqrt{2\pi}\ln\Lambda e^4 Z^2 n},
\end{aligned}
\tag{2.2}
$$

with $\ln\Lambda \approx 17$. The corresponding source terms are

$$
\begin{aligned}
S^n &= n_0 n \langle\sigma v\rangle_{iz},\\
S^m &= m_i u_0 S^n + m_i n_0 n \langle\sigma v\rangle_{cx}(u_0 - u),\\
S_i^E &= \frac{m_i}{m_0} S^n\Big(\frac{1}{2} m_0 u_0^2 + \frac{3}{2} T_0\Big) + m_i n_0 n \langle\sigma v\rangle_{cx}(u_0^2 - u^2),\\
S_e^E &= \frac{m_e}{m_0} S^n\Big(\frac{1}{2} m_0 u_0^2 + \frac{3}{2} T_0\Big) - S^n \phi_{iz}^{\text{eff}},\\
S_{i,e}^{E,ext} &= S_{i,e}^{E,ext-H} + S_{i,e}^{E,ext-RF},
\end{aligned}
\tag{2.3}
$$

with $T_0 = 2$ eV, $\phi_{iz}^{\text{eff}} = 13.6$ eV, and u_0 being the neutral velocity, which is assumed to be approximately equal to the thermal velocity $u_0 = \sqrt{T_0/m_0}$, with $m_0 = m_i$, where m_0 and m_i are the neutral and ion mass, respectively. The external source $S_{i,e}^{E,ext-H}$ is acting on the left side of the domain and given by a smoothed Heaviside function $h_0 H(x_0 - x)$ with h_0 chosen such that $\int_0^L S_{i,e}^{E,ext-H} dx = P_e$, where $P_e = 2.5$ MWm^{-1}. The details on the external RF source $S_{i,e}^{E,ext-RF}$ are discussed in Section 6. We ignore recombination, and use the polynomial approximation for the ionization rate coefficient:

$$
\langle\sigma v\rangle_{iz} = 3.0 \cdot 10^{-16}\, T_{e,[eV]}^2 / \left(3 + 0.01\, T_{e,[eV]}^2\right). \tag{2.4}
$$

The boundary conditions for the system (2.1) are

$$
\partial_x n_0 = \partial_x T_{i,e} = u = 0, \quad \text{at} \ \ x = 0, \tag{2.5}
$$

$$
\left.
\begin{aligned}
u &\geq \tilde{c}_s,\\
\tfrac{5}{2} n T_e u - n\chi_e \partial_x T_e &= \gamma_e T_e n u,\\
\Big(\tfrac{5}{2} n T_i + \tfrac{1}{2} m_i n u^2\Big) u - n\chi_i \partial_x T_i &= \gamma_i T_i n u,\\
-D_0 \partial_x n_0 &= -R n u,
\end{aligned}
\right\} \quad \text{at} \quad x = L,
\tag{2.6}
$$

with

$$
\tilde{c}_s = \sqrt{(T_e + T_i)/m_i}, \tag{2.7}
$$

where $\gamma_i = 2.5$, $\gamma_e = 5.5$, and $R = 1$. The boundary conditions at $x = L$ play a critical role in ensuring the physical consistency of the plasma model. In particular, the condition $u \geq \tilde{c}_s$, known as the Bohm criterion, see, e.g., [22, 23], enforces that the ion velocity entering the sheath must exceed the local sound speed, to allow for a stable sheath formation at the plasma-wall interface. This condition arises as the plasma shields electrons from recombining at the device walls at a higher rate than the ions, maintaining quasi-neutrality over the bulk of the plasma (see e.g., [24] for a derivation and further discussion). While the canonical Bohm criterion assumes an isothermal plasma regime (as defined above), variations arise under different plasma conditions, including ion temperature effects, collisionality, and sheath model assumptions. These modify the prefactors in the temperature in $\tilde{c}_s$ and reflect uncertainties or the need for higher fidelity transport descriptions, [22, 23]. A careful numerical treatment of the above boundary conditions is also essential for the stability and accuracy of the numerical solver, especially in operator-splitting schemes where boundary consistency across subsystems must be preserved as discussed in the next section.

3 Operator splitting scheme

We consider an operator splitting scheme for the temporal discretization of (2.1), which consists of a two-stage scheme, which we formally refer to as 'implicit' (diffusion sub-system) and 'explicit' (advection sub-system) stages. For the diffusion sub-system we use a semi-implicit temporal discretization, while the advection part is discretized using a SSP-RK3 (strong stability preserving Runge Kutta) method.

A crucial requirement for a stable time-splitting scheme is the well-posedness of the individual sub-systems. In our settings, nonlinear coupling arises at the SOL interface. The hyperbolic (advection) sub-system is particularly sensitive to correct boundary conditions due to its directional nature and the potential for characteristics entering or leaving the domain, requiring a careful analysis of how boundary conditions are enforced during the splitting, as discussed in Section 5. In contrast, the diffusion sub-system is more forgiving and admits classical well-posedness under standard boundary conditions. In the following, we appropriately separate the boundary coupling to ensure well-posedness and stability of each sub-system.

Stage 1 (implicit). In the first stage we solve the diffusion sub-system of equations:

$$\begin{aligned}
&\frac{\partial}{\partial t}n_0 - \frac{\partial}{\partial x}\left(D_0\frac{\partial}{\partial x}n_0\right) = -S^n,\\
&\frac{\partial}{\partial t}n = 0,\\
&\frac{\partial}{\partial t}(m_i nu) - \frac{\partial}{\partial x}(m_i n\mu\frac{\partial}{\partial x}u) = 0,\\
&\frac{\partial}{\partial t}\left(\frac{3}{2}nT_i + \frac{1}{2}m_i nu^2\right) - \frac{\partial}{\partial x}\left[n\chi_i\frac{\partial}{\partial x}T_i\right] = 0,\\
&\frac{\partial}{\partial t}\left(\frac{3}{2}nT_e\right) - \frac{\partial}{\partial x}\left(n\chi_e\frac{\partial}{\partial x}T_e\right) = 0,
\end{aligned} \tag{3.1}$$

subject to the following boundary conditions at $x = 0$:

$$\partial_x n_0 = \partial_x T_{i,e} = u = 0, \tag{3.2}$$

and at $x = L$:

$$\begin{aligned}
&\partial_x u = 0 \quad \text{if} \quad u > \tilde{c}_s \quad \text{and} \quad u = \tilde{c}_s \quad \text{if} \quad u \le \tilde{c}_s,\\
&\frac{5}{2}nT_e u - n\chi_e\partial_x T_e = \gamma_e T_e nu,\\
&\left(\frac{5}{2}nT_i + \frac{1}{2}m_i nu^2\right)u - n\chi_i\partial_x T_i = \gamma_i T_i nu,\\
&-D_0\partial_x n_0 = -Rnu.
\end{aligned} \tag{3.3}$$

It can be shown that with strictly positive diffusion coefficients the diffusion sub-system (3.1) supplemented with the mixed boundary conditions (3.2)–(3.3) is well-posed.

Stage 2 (explicit). The second stage of the scheme leads to the following hyperbolic system

$$\begin{aligned}
&\frac{\partial}{\partial t}n_0 = 0,\\
&\frac{\partial}{\partial t}n + \frac{\partial}{\partial x}(nu) = S^n,\\
&\frac{\partial}{\partial t}(m_i nu) + \frac{\partial}{\partial x}(m_i nu^2 + n(T_e + T_i)) = S^m,\\
&\frac{\partial}{\partial t}\left(\frac{3}{2}nT_i + \frac{1}{2}m_i nu^2\right) + \frac{\partial}{\partial x}\left[\left(\frac{5}{2}nT_i + \frac{1}{2}m_i nu^2\right)u\right] = S_i^E + S_i^{E,ext},\\
&\frac{\partial}{\partial t}\left(\frac{3}{2}nT_e\right) + \frac{\partial}{\partial x}\left(\frac{5}{2}nT_e u\right) = S_e^E + S_e^{E,ext},
\end{aligned} \tag{3.4}$$

subject to the following boundary conditions:

$$u = 0, \quad \text{at} \quad x = 0 \quad \text{and} \quad u \ge \tilde{c}_s, \quad \text{at} \quad x = L. \tag{3.5}$$

This represents a SOL flux tube with a physical target at $x = L$, where sheath boundary conditions are applied, and a symmetry condition at $x = 0$. We note that no additional boundary conditions are needed, as discussed in Section 5. A detailed analysis in Section 5 reveals, however, that boundary conditions (3.5) may lead to an ill-posed problem. We address how to mitigate this issue through appropriate modifications (cf. (5.3)) while still ensuring that the physical boundary conditions are satisfied.

We then use a semi-implicit discretization of (3.1) and an explicit discretization based on SSP-RK3 for (3.4). Since the latter follows a standard procedure and more details on the treatment of the boundary conditions are provided in Section 5, we present here a procedure for the time discretization of the former. In particular, for $T > 0$, $K \in \mathbb{N}$, $\Delta t = T/K$, $t^k = k\Delta t$, $k = 0, \ldots, K$, from the second equation in (3.1) we obtain $n^{k+1} = n^k = n(t^k)$ and

$$\frac{1}{\Delta t}\left(n_0^{k+1} - n_0^k\right) + \frac{\partial}{\partial x}\left(-D_0^k\frac{\partial}{\partial x}n_0^{k+1}\right) = -S^{n,k}, \tag{3.6a}$$

$$\frac{1}{\Delta t}m_i n^k\left(u^{k+1} - u^k\right) + \frac{\partial}{\partial x}\left(-m_i n^k\mu^k\frac{\partial}{\partial x}u^{k+1}\right) = 0, \tag{3.6b}$$

$$\frac{1}{\Delta t}n^{k+1}\left(\frac{3}{2}T_i^{k+1} + \frac{1}{2}m_i(u^{k+1})^2 - \frac{3}{2}T_i^k - \frac{1}{2}m_i(u^k)^2\right) \tag{3.6c}$$

$$+\frac{\partial}{\partial x}\left[-n^{k+1}\chi_i^k\frac{\partial}{\partial x}T_i^{k+1}\right] = 0, \tag{3.6d}$$

$$\frac{1}{\Delta t}n^{k+1}\left(\frac{3}{2}T_e^{k+1} - T_e^k\right) + \frac{\partial}{\partial x}\left(-n^{k+1}\chi_e^k\frac{\partial}{\partial x}T_e^{k+1}\right) = 0, \tag{3.6e}$$

where $S^{n,k} = n_0^k n^k\langle\sigma v\rangle_{iz}$. The corresponding boundary conditions at $x = 0$ (3.2) are discretized implicitly, and at $x = L$, (3.2), semi-implicitly using explicit updates for the coefficients $\chi_{i,e}$. Then, at each time step t^{k+1} the above system can be solved as a linear system of decoupled equations. First, having $n^k = n^{k+1}$ we perform an intermediate update, where we first solve for u^{k+1} in (3.6b), and then compute updates for T_i^{k+1} and T_e^{k+1} from (3.6c)–(3.6e), and evaluate $E_{i,e}^{k+1}$, respectively. Using those intermediate solutions, we proceed to Stage 2 to make a final update for $n^{k+1}, u^{k+1}, E_{i,e}^{k+1}$ using SSP-RK3 on (3.4)–(3.5). Lastly, using fully updated solutions, we solve (3.6a) to complete an update for n_0^{k+1}. Updating the neutral density at the final stage using the fully resolved solution was found to improve the resolution of strong boundary layers and enhance numerical stability.

4 Spatial discretization

We can express the system (2.1) in the general form

$$\frac{\partial \mathbf{u}}{\partial t} + \frac{\partial}{\partial x}\mathbf{F}(\mathbf{u}) - \frac{\partial}{\partial x}\left(\mathbf{D}(\mathbf{u})\frac{\partial}{\partial x}\mathbf{G}(\mathbf{u})\right) = \mathbf{S}(\mathbf{u}), \tag{4.1}$$

where $\mathbf{u} = [n_0, n, q, E_e, E_i]^T$ is a solution vector, $\mathbf{D}(\mathbf{u}) = \text{diag}\,[D_0,\ 0,\ n\mu,\ n\chi_i,\ n\chi_e]$, $\mathbf{S}(\mathbf{u}) = \left[-S^n,\ S^n,\ S^m/m_i,\ S_i^E + S_i^{E,ext},\ S_e^E + S_e^{E,ext}\right]^T$, and $\mathbf{F}(\mathbf{u})$ is a vector corresponding to the advection fluxes in (3.4). We also introduce the Jacobian $\mathbf{J}(\mathbf{u})$ of $\mathbf{F}(\mathbf{u})$

$$\mathbf{J}(\mathbf{u}) = \begin{bmatrix} 0 & 0 & 0 & 0 & 0 \\ 0 & 0 & 1 & 0 & 0 \\ 0 & -\frac{2}{3}u^2 & \frac{4}{3}u & \frac{2}{3m_i} & \frac{2}{3m_i} \\ 0 & \frac{2}{3}m_i u^3 - \frac{5}{3}\frac{E_i u}{n} & -u^2 m_i + \frac{5}{3}\frac{E_i}{n} & \frac{5}{3}u & 0 \\ 0 & -\frac{5}{3}\frac{E_e u}{n} & \frac{5}{3}\frac{E_e}{n} & 0 & \frac{5}{3}u \end{bmatrix} \tag{4.2}$$

with the eigenvalues $\lambda = \left\{0, u, u - c_s, u + c_s, \frac{5}{3}u\right\}$, where

$$c_s = \sqrt{5(p_i + p_e)/(3m_i n)} = \sqrt{5(T_i + T_e)/(3m_i)}. \tag{4.3}$$

We note that the speed of sound c_s above obtained from the analysis of the model differs from the modeling choice $\tilde{c}_s$ defined in (2.7) by a factor $\sqrt{5/3}$. In Section 5, we discuss the implications of this choice on the prescription of boundary conditions and the well-posedness of the system.

For spatial discretization, we employ a nodal DG FEM using local DG (LDG) FEM discretization with stabilized central flux for the diffusion sub-system, see, e.g., [25–27], and the local Lax-Friedrichs flux (4.4) to approximate $\mathbf{F}(\mathbf{u})$. Since the DG discretization of the diffusion subsystem (3.1) is relatively straightforward, we focus on the discretization details and boundary treatment for (3.4).

Let $0 = x_{1/2} < x_{3/2} < \cdots < x_{N-1/2} < x_{N+1/2} = L$, be a partition of the spatial domain $\Omega = [0, L]$, and for $j = 1, \ldots, N$, let $E_j = (x_{j-1/2}, x_{j+1/2})$ and $h_j = (x_{j+1/2} - x_{j-1/2})$. Let $P_k(E_j)$ be the space of vector-valued polynomial functions of order k on E_j. We approximate $\mathbf{u}$ by a piece-wise defined function $\mathbf{u}_h$, such that $\mathbf{u}_h|_{E_j} \in P_k(E_j)$, that is, the restriction of $\mathbf{u}_h$ to E_j lies in the local space $P_k(E_j)$. At interior element edges $x_{\ell+1/2}$, $\ell = 1, \ldots, N-1$, we approximate $\mathbf{F}(\mathbf{u})|_{x=x_{\ell+1/2}}$ with a numerical flux:

$$\hat{\mathbf{F}}_{\ell+1/2}\left(\mathbf{u}_h^\ell, \mathbf{u}_h^{\ell+1}\right) = \{\mathbf{F}(\mathbf{u}_h)\}_{\ell+1/2} + \frac{\alpha(\mathbf{u}_h^\ell, \mathbf{u}_h^{\ell+1})}{2}[[\mathbf{u}_h]]_{\ell+1/2}, \tag{4.4}$$

where $\alpha(\mathbf{u}_h^\ell, \mathbf{u}_h^{\ell+1}) = \max\{\left|\frac{\partial \mathbf{F}}{\partial \mathbf{u}}(\mathbf{u}_h^\ell)\right|, \left|\frac{\partial \mathbf{F}}{\partial u}(\mathbf{u}_h^{\ell+1})\right|\}$ (local Lax-Friedrichs flux). Note $\{\cdot\}_{\ell+1/2}$ and $[[\cdot]]_{\ell+1/2}$ represent the average and jump operators, respectively:

$$\{\mathbf{F}(\mathbf{u}_h)\}_{\ell+1/2} = \frac{1}{2}\left[\mathbf{F}\left(\mathbf{u}_h^\ell|_{x=x_{\ell+1/2}}\right) + \mathbf{F}\left(\mathbf{u}_h^{\ell+1}|_{x=x_{\ell+1/2}}\right)\right],$$
$$[[\mathbf{u}_h]]_{\ell+1/2} = \mathbf{u}_h^\ell|_{x=x_{\ell+1/2}} - \mathbf{u}_h^{\ell+1}|_{x=x_{\ell+1/2}}.$$

Here and in what follows, we use the subscript h to indicate the discretized solution and discrete quantities.

Prescription of the boundary fluxes

Next, we discuss the set-up of the boundary fluxes $\hat{\mathbf{F}}_{1/2}$ and $\hat{\mathbf{F}}_{N+1/2}$ for the hyperbolic subsystem (3.4), ensuring that the boundary conditions (3.5) are enforced in a stable and consistent manner. For simplicity, let $\mathbf{u}_h^-$ and $\mathbf{u}_h^+$ denote the values at the left and right side of the interface, respectively. Then, to define $\hat{\mathbf{F}}_{1/2}$ and $\hat{\mathbf{F}}_{N+1/2}$ in (4.4), we need to determine the unknown values $\mathbf{u}_h^-$ at $x = 0$ and $\mathbf{u}_h^+$ at $x = L$, respectively. At the left boundary $x = 0$ we have $u = 0$ (3.5), and thus we set $\{u_h\} = \frac{u_h^+ + u_h^-}{2} = 0$, which implies $u_h^+ = -u_h^-$. To determine the values for other variables we set $[\![n_h]\!] = 0$ (i.e, $n_h^+ = n_h^-$) and $[\![p_{h,i,e}]\!] = 0$ (i.e., $p_{h,i,e}^+ = p_{h,i,e}^-$), which yields conservation properties for the hyperbolic system. It directly follows that $q_h^+ = -q_h^-$ and $E_{h,i,e}^+ = E_{h,i,e}^-$ and $\hat{F}_{1/2}(n_h^-, n_h^+) = \hat{F}_{1/2}(E_{h,i}^-, E_{h,i}^+) = \hat{F}_0(E_{h,e}^-, E_{h,e}^+) = 0$ at $x = 0$, and

$$\hat{F}_{1/2}(q_h^-, q_h^+) = n_h^+(u_h^+)^2 + \frac{p_{h,i}^+ + p_{h,e}^+}{m_i} - \alpha_h q_h^+.$$

At the right boundary $x = L$ in accordance with the boundary conditions (3.5) we set $\{u_h\} = c_{s,h}$ (or $\{u_h\} = \tilde{c}_{s,h}$) if $c_{s,h} \geq u_h$ (see Section 5 for more details) and as before $[\![n_h]\!] = 0$, $[\![p_{h,i,e}]\!] = 0$. Here, $c_{s,h}$ and $\tilde{c}_{s,h}$ are discretized versions of (4.3) and (2.7), respectively. Then, $u_h^+ = 2c_{s,h} - u_h^-$, $n_h^+ = n_h^-$, $p_{h,i,e}^+ = p_{h,i,e}^-$ and $q_h^+ = 2c_{s,h}n_h^- - q_h^-$, and the boundary fluxes then become

$$\begin{aligned}
\hat{F}_{N+1/2}(n_h^-, n_h^+) =& c_{s,h}n_h^-, \\
\hat{F}_{N+1/2}(q_h^-, q_h^+) =& F_2^- + (q_h^- - c_{s,h}n_h^-)(\alpha_h - 2c_{s,h}), \\
\hat{F}_{N+1/2}(E_{h,i}^-, E_{h,i}^+) =& c_{s,h}\left(E_{h,i}^- + p_{h,i}^-\right) \\
&+ m_i c_{s,h} n_h^- \left(c_{s,h} - u_h^-\right)\left(2c_{s,h} - u_h^- - \alpha_h\right), \\
\hat{F}_{N+1/2}(E_{h,e}^-, E_{h,e}^+) =& 5/3 c_{s,h} E_{h,e}^-,
\end{aligned}$$

where F_2 corresponds to the hyperbolic flux in the second equation of (3.4).

5 Study of the boundary conditions

We analyze (3.4), which can be expressed as

$$\frac{\partial \mathbf{u}}{\partial t} + \frac{\partial}{\partial x}\mathbf{F}(\mathbf{u}) = 0, \tag{5.1}$$

where $\mathbf{u} = [n, q, E_e, E_i]^T$ and $\mathbf{F}(\mathbf{u})$ is the corresponding advection flux. For simplicity, we omit the n_0 term as it yields no contribution to the flux, and by slight abuse of notation use the same symbols for $\mathbf{u}$, $\mathbf{F}$ and the Jacobian $\mathbf{J}(\mathbf{u})$. To verify the correctness of the boundary conditions, we linearize and diagonalize the system around a reference state to obtain characteristic variables. Analyzing the number of incoming and outgoing characteristic waves determines the number of boundary conditions required for well-posedness of the linearized system and offers a necessary condition and guidance for proper boundary specification in the nonlinear case (3.4).

We diagonalize the system around a constant reference state, which by a slight abuse of notation we denote again by $\mathbf{u}$, with a perturbation $\hat{\mathbf{u}}$:

$$\frac{\partial}{\partial t}\hat{\mathbf{u}} + \mathbf{A}\frac{\partial}{\partial x}\hat{\mathbf{u}} = 0, \tag{5.2}$$

where $\mathbf{A} = \mathbf{J}(\mathbf{u}) = \mathbf{X}\mathbf{\Lambda}\mathbf{X}^{-1}$, $\mathbf{\Lambda} = \mathrm{diag}[u, u - c_s, u + c_s, \frac{5}{3}u]$, $\mathbf{X}$ is the matrix of corresponding eigenvectors.

Next, we analyze the linearized boundary conditions for (5.2). At $x = 0$, $u = 0$ and there is one positive eigenvalue corresponding to one incoming wave, and imposing $u = 0$ is sufficient, as argued below. On the other hand, at $x = L$ for $u < c_s$ there is only one negative eigenvalue and one boundary condition needs to be imposed, whereas for $u > c_s$ all eigenvalues are positive and no boundary conditions needed. We observe that for $\tilde{c}_s < u < c_s$ there is a discrepancy between the boundary conditions in (3.5) and the ones arising from the linearization analysis. The former suggests not to impose any boundary conditions for $u > \tilde{c}_s$, potentially leading to an ill-posed and numerically unstable problem. Therefore, we propose a modification of the boundary conditions that guarantee the well-posedness and still fulfill the condition $u \geq \tilde{c}_s$ in (2.6). In particular, we suggest imposing at $x = L$ either

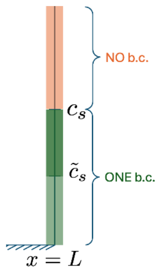

$$u = c_s \quad \text{or} \quad u = \tilde{c}_s, \quad \text{whenever} \quad u < c_s. \tag{5.3}$$

The corresponding linearization of those conditions leads to $\mathbf{a}^T\hat{\mathbf{u}} = 0$ or $\mathbf{b}^T\hat{\mathbf{u}} = 0$, where $\mathbf{a}$ and $\mathbf{b}$ are the vectors obtained from the linearization of $(u^2 - c_s^2)n = 0$ or $(u^2 - \tilde{c}_s^2)n = 0$, which is equivalent to imposing $u = c_s$ or $u = \tilde{c}_s$ whenever $u < c_s$, respectively. Our goal is to show that the chosen boundary conditions lead to a well-posed problem (5.2). From [28, Theorem 8.1.1], this requires showing that the incoming characteristic waves can be expressed in terms of the outgoing ones.

Then, using the eigensystem of $\mathbf{A}$ and introducing a vector of characteristic variables $\mathbf{w} = [w_1, w_2, w_3, w_4]^T = \mathbf{X}^{-1}\hat{\mathbf{u}}$ we can transform (5.2) to

$$\frac{\partial}{\partial t}\mathbf{w} + \mathbf{\Lambda}\frac{\partial}{\partial x}\mathbf{w} = 0.$$

For $x = 0$ we have $u = 0$ or equivalently $q = 0$, which leads to $\hat{q} = 0$, and using that $\hat{\mathbf{u}} = \mathbf{X}\mathbf{w}$ and assuming $c_s \neq 0$, we obtain

$$0 = \hat{q}(0) = (uw_1 + (u - c_s)w_2 + (u + c_s)w_3)\,|_{x=0},$$

and since $u|_{x=0} = 0$ we obtain that an incoming wave is expressed via outgoing, i.e., $w_2 = w_3$ on $x = 0$. Similarly, at $x = L$ solving $\mathbf{a}^T\hat{\mathbf{u}} = \mathbf{a}^T\mathbf{X}\mathbf{w} = 0$ leads to

$$3u^2w_1 - \left(5\,c_s^2 + 6\,c_s u - 3\,u^2\right)w_2 - \left(5\,c_s^2 - 6\,c_s u - 3\,u^2\right)w_3 = 0,$$

and inserting $u = c_s \neq 0$ leads to $w_2 = \frac{3}{8}w_1 + \frac{1}{2}w_3$, where the incoming wave is expressed via outgoing ones. Analogously, if instead $\mathbf{b}^T\hat{\mathbf{u}} = \mathbf{b}^T\mathbf{X}\mathbf{w} = 0$ at $x = L$, we have

$$u^2w_1 - \left(c_s^2 + 2\,c_s u - u^2\right)w_2 - \left(c_s^2 - 2\,c_s u - u^2\right)w_3 = 0.$$

Since, $u = \tilde{c}_s < c_s$ it follows that $\left(c_s^2 + 2\,c_s u - u^2\right) \neq 0$ and, hence we can express w_2 in terms of w_1 and w_3. This proves that the set of boundary conditions (5.3) ensures the well-posedness of (5.2), and provides necessary conditions for the well-posedness of the nonlinear system (3.4).

6 Numerical results

We consider the domain $\Omega = [0, L]$ with $L = 30$ (m), discretized with a non-uniform mesh with a finer mesh refinement towards the right boundary $x = L$ to resolve a steep boundary layer. We use second order polynomials and 1113 elements with the mesh sizes $\Delta x_{max} = 0.0175$ (m), $\Delta x_{min} = 0.0038$ (m) and a time step $\Delta t = 10^{-7}$. For initialization we use flat initial profiles for density and temperatures, $n^0 = 8 \cdot 10^{18}$ m^{-3} and $T_{i,e}^0 = 20$ (eV). We use a quadratic profile for the initial condition for the velocity, $u^0 = ax^2$, $a = 3.4643 \cdot 10^4$, and the neutrals are initialized as $n_0^0 = 0$ (1/m^3). A 50 MWm^2 power flux is included via $S_{i,e}^E$, split equally between ions and electrons, from $x = 0$ to $x = 10$ (m). The profile is calculated using an approximate analytic expression for a smoothed Heaviside step function $H = A/(1 + \exp(2k(x - x_0)))$, where $A = 2.5$ MWm^{-1}, $k = 0.8$ is the width of the transition region, and $x_0 = 10$ (m). The parameters are set-up as follows: $R = 1$, $\gamma_i = 2.5$, $\gamma_e = 5.5$, $\langle\sigma v\rangle_{cx} = 3 \cdot 10^{-14}$ (m^{3}s^{-1}), $u_0 = 10^4$ (m/s), $T_0 = 2$ (eV), $m_i = m_0 = 5.34 \cdot 10^{-27}$ (kg), $m_e = 9.11 \cdot 10^{-31}$ (kg), $\phi_{iz}^{\mathrm{eff}} = 13.6$ (eV), $\langle\sigma v\rangle_{iz}$ is defined as in (2.4), and the remaining parameters $D_0, \tau_{i,e}, \chi_{i,e}, \mu$ are defined in (2.2). In Figure 1 we depict solutions at a terminal time $t = 0.004$ (s). We observe that numerical discretization provides a stable approximation of the boundary conditions and boundary layer formed at the right boundary in neutrals profiles.

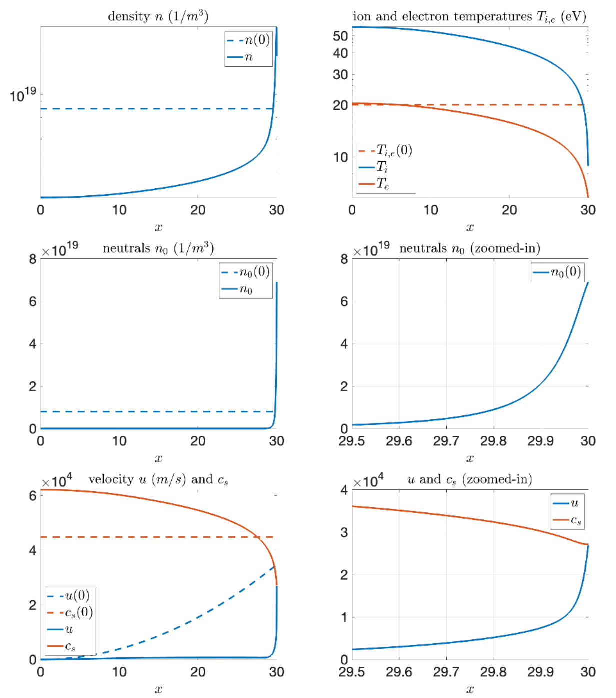

Figure 1. Snapshots of the solutions at initial (dashed line) and final time, $t = 0.004$ (s) (solid line).

RF source term

Next, we consider settings with added RF source. We used a simple, one-dimensional full-wave cold plasma solver with present day tokamak relevant RF parameters to approximate a power deposition profile in the domain. A Gaussian current density profile centered at $x = 0$ was used to drive a plasma wave, which was artificially damped close to $x = 0$ to simulate wave power absorption. Equilibrium plasma transport profiles from the previous simulations provided the initial conditions, and the additional external heating source $S_{i,e}^{E,ext-RF}$ was added for a duration of $t = 10^{-7}$(s), before the simulation was again run towards a quasi stationary solution. The current density magnitude was scaled to provide enough power to observe a visible effect, and the power absorption was calculated using $P(x) = E(x)^2\sigma(x)$ Wm^{-3}, where $\sigma(x)$ is the plasma conductivity, $\sigma(x) = 4/3\sqrt{2\pi}\ln\Lambda\sqrt{m_e}Ze^2/((4\pi\epsilon_0)^2T_e^{3/2})$ Sm^{-1}. Assuming a flux tube cross section unit area $A = 1.0$ m^2, we can determine a power absorption profile over the one-dimensional domain that becomes an additional external source term for $E_{i,e}$. We found the total power absorbed over the domain to be approximately 37 MW. The snapshots of the solutions are depicted on Figure 2. We observe a change in the profiles close to the right boundary as the energy spreads across the domain, particularly in the velocity, which highlights material flow reversing in this region as the plasma equilibrates again. Although this result is not physical given the range of assumptions, it presents an example of how RF wave fields can impact far-SOL fluid transport.

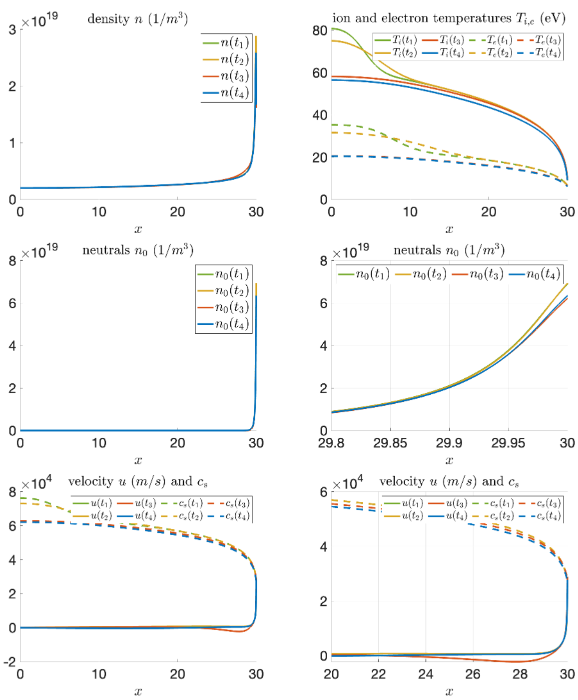

Figure 2. Snapshots of the solutions at different time steps ($t_1 = 4\cdot10^{-7}$ (s), $t_2 = 8\cdot10^{-7}$ (s), $t_3 = 8\cdot10^{-5}$ (s), $t_4 = 4.14\cdot10^{-4}$ (s)) after the RF source was added to the system. The initial condition was taken as a solution from the previous example at $t = 0.004$ (s).

7 Conclusion and discussion

We have introduced an operator splitting method with DG discretization for a Braginskii-type plasma fluid model in the far SOL plasma. The approach effectively addresses strong coupling between diffusion and advection terms, especially at boundaries, using a two-stage splitting scheme. We provided a detailed analysis on the appropriate specification of the boundary conditions for each sub-system. Numerical results confirm the method's stability, laying the groundwork for future studies of complex plasma dynamics involving RF heating.

Acknowledgments

This manuscript has been authored in part by UT-Battelle, LLC, under contract DE-ACO5-000R22725. Olena Burkovska, Rhea Barnett, Christopher Vogl, Jeremy Lore and Cory Hauck acknowledge the support from the US DOE Office of Fusion Energy Sciences and DOE Advanced Scientific Computing Research as part of the SciDAC program. This work was also performed in part under the auspices of the U.S. Department of Energy by Lawrence Livermore National Laboratory under Contract DE-AC52-07NA27344, LLNL-PROC-2007576. We would like to thank Dr. Paul Bonoli for constant encouragement and interest in this work.

References

[1] R. Schneider, X. Bonnin, K. Borrass, D.P. Coster, H. Kastelewicz, D. Reiter, V.A. Rozhansky, B.J. Braams, Plasma Edge Physics with B2-Eirene, Contributions to Plasma Physics **46**, 3 (2006). https://doi.org/10.1002/ctpp.200610001

[2] S. Wiesen, D. Reiter, V.K. et al., The new SOLPS-ITER code package, Journal of Nuclear Materials **463**, 480 (2015). https://doi.org/10.1016/j.jnucmat.2014.10.012

[3] T. Rognlien, X. Xu, A. Hindmarsh, Application of Parallel Implicit Methods to Edge-Plasma Numerical Simulations, Journal of Computational Physics **175**, 249 (2002). https://doi.org/10.1006/jcph.2001.6944

[4] R. Simonini, G. Corrigan, G. Radford, J. Spence, A. Taroni, Models and Numerics in the Multi-Fluid 2-D Edge Plasma Code EDGE2D/U, Contributions to Plasma Physics **34**, 368 (1994). https://doi.org/10.1002/ctpp.2150340242

[5] G. Giorgiani, S. Fernández-Méndez, A. Huerta, Hybridizable Discontinuous Galerkin with degree adaptivity for the incompressible Navier–Stokes equations, Computers & Fluids **98**, 196 (2014). https://doi.org/10.1016/j.compfluid.2014.01.011

[6] G. Giorgiani, H. Bufferand, G. Ciraolo, P. Ghendrih, F. Schwander, E. Serre, P. Tamain, A hybrid discontinuous Galerkin method for tokamak edge plasma simulations in global realistic geometry, Journal of Computational Physics **374**, 515 (2018). https://doi.org/10.1016/j.jcp.2018.07.028

[7] A. Kukushkin, H. Pacher, V. Kotov, G. Pacher, D. Reiter, Finalizing the ITER divertor design: The key role of SOLPS modeling, Fusion Engineering and Design **86**, 2865 (2011). https://doi.org/10.1016/j.fusengdes.2011.06.009

[8] C. Sang, H. Guo, P. Stangeby, L. Lao, T. Taylor, SOLPS analysis of neutral baffling for the design of a new diverter in DIII-D, Nuclear Fusion **57**, 056043 (2017). https://doi.org/10.1088/1741-4326/aa6548

[9] R. Davies, Y. Feng, D. Boeyaert, J.C. Schmitt, M.J. Gerard, K.A. Garcia, O. Schmitz, B. Geiger, S.A. Henneberg, A semi-automated algorithm for designing stellarator divertor and limiter plates and application to HSX, Nuclear Fusion **64**, 126044 (2024). https://doi.org/10.1088/1741-4326/ad8017

[10] T. Lunt, H. Zohm, A. Herrmann, A. Kallenbach, M. Dunne, Y. Feng, R. Neu, M. Wischmeier, Proposal of an alternative upper divertor in ASDEX Upgrade supported by EMC3-EIRENE simulations, Nuclear Materials and Energy **12**, 1037 (2017). https://doi.org/10.1016/j.nme.2016.12.035

[11] J. Rapp, L. Owen, X. Bonnin, J. Caneses, J. Canik, C. Corr, J. Lore, Transport simulations of linear plasma generators with the B2.5-Eirene and EMC3-Eirene codes, Journal of Nuclear Materials **463**, 510 (2015). https://doi.org/10.1016/j.jnucmat.2014.12.058

[12] D. D'Ippolito, J. Myra, J. Rogers, K. Hill, J. Hosea, R. Majeski, G. Schilling, J. Wilson, G. Hanson, A. England et al., Analysis of RF sheath interactions in TFTR, Nuclear Fusion **38**, 1543 (1998). https://doi.org/10.1088/0029-5515/38/10/311

[13] G. Hanson, J. Wilgen, C. Lau, Y. Lin, G. Wallace, S. Wukitch, Scrape-off layer reflectometer for Alcator C-Mod, Review of Scientific Instruments **79**, 10D918 (2008). https://doi.org/10.1063/1.2966460

[14] C. Lau, Y. Lin, G.R. Hanson, G. Wallace, S.J. Wukitch, B. LaBombard, R. Ochoukov, S. Shiraiwa, J. Terry, J. Wilgen, LH and ICRF driven scrape-off-layer density modifications and their impact on LH coupling on Alcator C-Mod, AIP Conference Proceedings **1580**, 410 (2014). https://doi.org/10.1063/1.4864575

[15] W. Zhang, Y. Feng, J.M. Noterdaeme, V. Bobkov, L. Colas, D. Coster, T. Lunt, R. Bilato, J. Jacquot, R. Ochoukov et al., Modelling of the ICRF induced $E \times B$ convection in the scrape-off-layer of ASDEX Upgrade, Plasma Physics and Controlled Fusion **58**, 095005 (2016). https://doi.org/10.1088/0741-3335/58/9/095005

[16] L. Colas, G. Urbanczyk, M. Goniche, J. Hillairet, J.M. Bernard, C. Bourdelle, N. Fedorczak, C. Guillemaut, W. Helou, V. Bobkov et al., The geometry of the ICRF-induced wave–SOL interaction. A multi-machine experimental review in view of the ITER operation, Nuclear Fusion **62**, 016014 (2021). https://doi.org/10.1088/1741-4326/ac35f9

[17] M. Martin, W. Gekelman, B. Van Compernolle, P. Pribyl, T. Carter, Experimental Observation of Convective Cell Formation due to a Fast Wave Antenna in the Large Plasma Device, Phys. Rev. Lett. **119**, 205002 (2017). https://doi.org/10.1103/PhysRevLett.119.205002

[18] M. Bécoulet, L. Colas, S. Pécoul, J. Gunn, P. Ghendrih, A. Bécoulet, S. Heuraux, Edge plasma density convection during ion cyclotron resonance heating on Tore Supra, Physics of Plasmas **9**, 2619 (2002). https://doi.org/10.1063/1.1472501

[19] P.C. Stangeby, The plasma boundary of magnetic fusion devices (CRC Press, 2000)

[20] P. Stangeby, J. Lore, R. Pitts, J. Canik, X. Bonnin, A reduced model for the ITER divertor based on SOLPS solutions for ITER Q = 10 baseline conditions: A. identifying options for the control parameters, Nuclear Fusion **63**, 016016 (2022). https://doi.org/10.1088/1741-4326/ac9916

[21] S.I. Braginskii, Transport processes in a plasma, Reviews of Plasma Physics **1**, 205 (1965).

[22] K.U. Riemann, The Bohm criterion and sheath formation, Journal of Physics D: Applied Physics **24**, 493 (1991). https://doi.org/10.1088/0022-3727/24/4/001

[23] Y. Li, B. Srinivasan, Y. Zhang, X.Z. Tang, Bohm Criterion of Plasma Sheaths away from Asymptotic Limits, Phys. Rev. Lett. **128**, 085002 (2022). https://doi.org/10.1103/PhysRevLett.128.085002

[24] F.F. Chen, Introduction to Plasma Physics and Controlled Fusion (Springer, 2016)

[25] J.S. Hesthaven, T. Warburton, Nodal discontinuous Galerkin methods: algorithms, analysis, and applications (Springer, 2008)

[26] B. Cockburn, C.W. Shu, The local discontinuous Galerkin method for time-dependent convection-diffusion systems, SIAM Journal on Numerical Analysis **35**, 2440 (1998).

[27] Y. Xu, C.W. Shu, Local discontinuous Galerkin methods for high-order time-dependent partial differential equations, Communications in Computational Physics **7**, 1 (2010). https://doi.org/10.1137/S0036142997316712

[28] B. Gustafsson, H.O. Kreiss, J. Oliger, Time dependent problems and difference methods, Vol. 2 (Wiley Online Library, 2013)